AERES: Thermodynamic and Economic Optimization Software for Hybrid Solar–Waste Heat Systems

Icaro Figueiredo Vilasboas [1],*, Victor Gabriel Sousa Fagundes dos Santos [2], Vinicius Oliveira Braz de Morais [1], Armando Sá Ribeiro, Jr. [3] and Julio Augusto Mendes da Silva [4]

[1] Industrial Engineering Program (PEI), Federal University of Bahia, Salvador 40210-630, Brazil; viniciusmorais@jsglobal.com.br

[2] Department of Electrical and Computer Engineering (DEEC), Federal University of Bahia, Salvador 40210-630, Brazil; victor.sousa@ufba.br

[3] Department of Construction and Structures (DCE), Federal University of Bahia, Salvador 40210-630, Brazil; asrj@ufba.br

[4] Department of Mechanical Engineering (DEM), Federal University of Bahia, Salvador 40210-630, Brazil; julio.silva@ufba.br

* Correspondence: icaro.vilasboas@ufba.br

Abstract: Heliothermic technologies are affected by their low density, intermittence and low economic competitiveness. Hybrid solar–waste heat power systems can increase plant conversion efficiency and power generation while reducing intermittence. This study focused on the development of software (AERES) to economically optimize hybrid solar–waste heat power systems in terms of technology selection, sizing, operating conditions and power block characteristics. The technologies considered for algorithm selection were (i) heat exchangers that recover a wide range of waste heat sources, (ii) non-concentrating and concentrating solar collectors (a flat plate, an evacuated tube, a linear Fresnel and a parabolic trough), (iii) organic Rankine cycle power blocks and (iv) storage tanks (direct thermal storage systems). The last two technologies were represented by surrogate models so that a large number of decision variables could be optimized simultaneously. The optimization considered local climate conditions hourly to provide irradiation, local temperature and wind speed. The case studies indicated that optimized ORCs for waste heat recovery are economically competitive, reaching internal rates of return (IRRs) of 44%, 39% and 34% for a waste heat of 50 MWt at 350 °C, 300 °C and 250 °C, respectively. On the other hand, heliothermic technologies were not selected by the algorithm and provided non-competitive results for the analyzed cases.

Keywords: solar thermal; hybrid solar power; heliothermic power; waste heat recovery; thermodynamic and economic optimization

1. Introduction

The progressive increase in global energy consumption and the need to reduce the greenhouse effect are driving researchers to seek more efficient processes and renewable energy sources. In this context, solar energy can be considered inexhaustible as it emits 1.7×10^8 GW of power to the earth's surface [1], which represents more than 5500 times the expected global capacity in 2050 [2].

The main challenges for the implementation of solar plants are their low energy density [3], the low capacity factor of generating units [4] and the geographic dependence on areas with high levels of solar radiation [5]. Solar thermal power plants (STPPs) can use energy storage systems to increase their capacity factors while decreasing the effects of solar intermittence [6]. Furthermore, solar concentrators can increase the global energy efficiency of power systems by increasing the operating temperature and reducing thermal losses in the receivers [7,8].

The hybridization of power systems through the use of solar thermal power and waste heat recovery to increase the power generation and efficiency and reduce the specific greenhouse gas emissions of existent plants is a relevant subject that has been addressed in several works. Mendecka et al. [9] applied an exergo-ecological analysis to compare a solar–waste heat power plant and a gas-integrated waste heat power plant. Their results indicated that despite its ecological advantages, the solar–waste heat power plant had higher exergetic costs. Franchini et al. [10] compared a solar Rankine cycle (SRC) and an integrated solar Rankine cycle (ISRC) that combined solar collectors with waste heat that was recovered from gas turbine gases. Their results showed that the solar-to-electric efficiency increased by 4.8% when ISRC was applied using parabolic trough collectors and by 2.3% when the integrated system used solar tower collectors. Rashid et al. [11] compared two configurations of hybrid solar–natural gas power plants: (i) grid-level hybridization, when two independent plants generated electricity for the same energy grid and (ii) plant-level hybridization, when two heat sources (solar and waste gases) were used as the supply for the same power plant. The plant-level unit showed several advantages over the grid-level configuration, such as solar-to-electric efficiency, solar fraction and emission levels of 33%, 20% and 0.43 tonne/MWh, respectively, compared to 31%, 12% and 0.54 tonne/MWh for the grid-level plant, respectively. Chen et al. [12] proposed a steam cycle that was supplied by a hybrid solar and solid waste plant. With this design, the solar energy produced 1.17 MWe of net energy with a solar-to-energy efficiency of about 21.6% and a levelized cost of energy (LCOE) of 0.12 USD/kWh. Similarly, Arabkoohsar and Sadi [13] presented a hybrid solar–waste incineration power plant and their results revealed an LCOE of 0.82 USD/kWh. According to [13], these results were more competitive than those from traditional heliothermic plants (1.2 USD/kWh). Han et al. [14], on the other hand, proposed the integration of non-concentrating solar collectors to preheat air in boilers. Their results revealed a slight increase in energy efficiency (0.57%) and a decrease of 37% in exergy loss using the air preheating process.

The thermodynamic and economic optimization of power plants is complex as it requires the simultaneous optimization of configuration, sizing and operational parameters. Integrated solar combined cycles (ISCCs) provide a wide variety of possible structures, as presented by Behar et al. [15], e.g., (i) solar collectors as intermediate-pressure vapor generators in gas turbine waste heat recovery power plants [16], (ii) solar collectors in series with biomass gas turbine exhaust to heat the heat transfer fluid [17] and (iii) solar collectors used to increase the temperature of geothermal sources in order to produce power and hot water for domestic use [18]. Alirahmi et al. [18] proposed a multi-objective optimization of a multi-generation hybrid solar and geothermal plant. This design was optimized in terms of the exergy efficiency and specific cost and resulted in 29.95% and 129.7 USD/GJ, respectively. Coutinho et al. [19] proposed a hybrid solar–natural gas power plant for generation-scale distributed power (<100 kWe) using a constant direct normal irradiance of 1600 kWh/m^2 yr. The power block consisted of a Brayton topping cycle and a Rankine bottoming cycle. The LCOE resulting from this plant was 0.179 USD/kWh. Elmorsy et al. [20] performed exergy-based optimization on a structure composed of a gas turbine, waste heat recovery (WHR) and a direct steam linear Fresnel reflector (LFR). A separated backpressure steam turbine was supplied with steam from collectors and its outlet was connected to the WHR system and the low-pressure turbine. The authors indicated that an interactive optimization could lead to an LCOE of 40.0 USD/MWh with specific cost of 1088 USD/kW. Rovira et al. [21] presented a combined solar thermal and gas turbine with a WHR system and vapor injection. The solar field system was used to provide additional vapor for the turbine. Their results revealed no significant variations in the LCOE (~93 EUR/MWh) when the solar field was included in the structure. In contrast, a considerable difference in LCOE was obtained in the results presented in [20], indicating that hybridization results are very dependent on the chosen configuration, location and assumptions.

This work presents the methodology that was used to create a software to perform economic optimization for hybrid systems, which could be composed of solar fields (flat

plate, evacuated tube, linear Fresnel or parabolic trough), WHR or optimized power blocks (ORCs). The system configuration, operational parameters and sizing were simultaneously optimized for the local climate and the temperature, power and type of the waste heat.

2. Hybrid Solar–Waste Heat Power System

Four solar thermal technologies were considered as possible components for the solar field, together with heat exchangers for up two waste heat sources: (i) a flat plate collector, (ii) a evacuated tube collector, (iii) a linear Fresnel reflector and (iv) a parabolic trough collector.

Figure 1 shows the hybrid solar field (HSF) that was available for the algorithm selection of technologies and configuration. Four of the six numerated boxes represent solar collectors and two represent heat exchangers to make use of the waste heat sources. The solar collector and heat exchanger positions were not fixed and depended on their operational temperature. The solar hybrid power plant could use (or not) a direct thermal storage system (TES) to store the excess of energy from the HSF and supply the power block (PB) when the energy provided by the HSF was less than required.
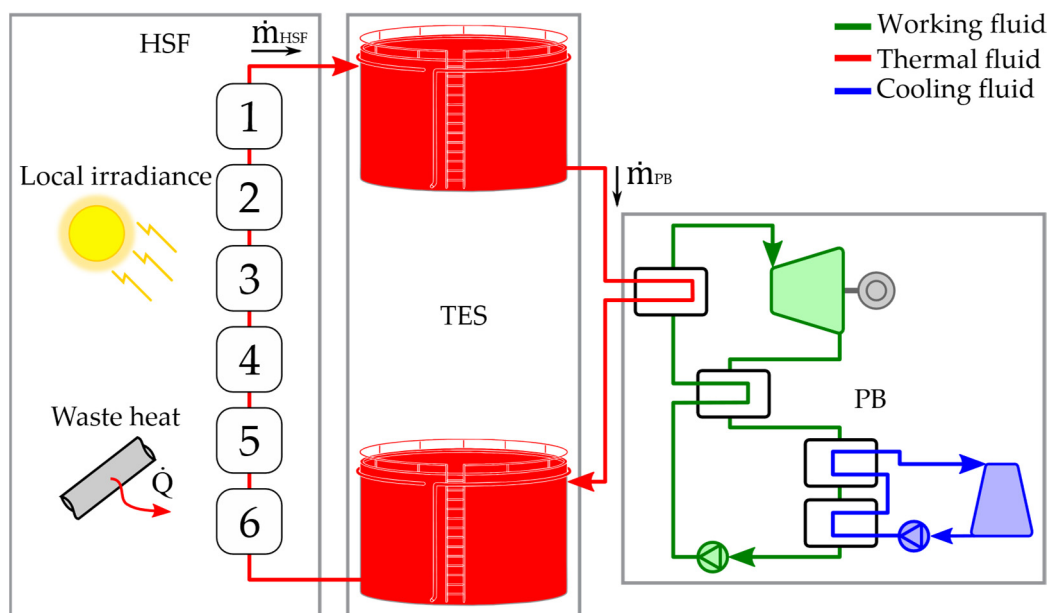
Figure 1. General hybrid solar power plant scheme with a hybrid solar field (**left**), power block (**right**) and direct thermal energy storage system (**center**).

3. Methodology

Both heat exchangers and solar collectors were modeled using Thermal Engineering Systems in the Python (TESPy) toolkit [22]. The TES energy loss and ORC power block were modeled using a surrogate model approach, which was developed in Scikit-learn [23]. The thermophysical properties were obtained using the CoolProp [24] python wrapper. The meteorological data from specific regions were obtained from the NREL weather database [25]. The energy and mass balances were evaluated in steady-state every hour. The potential and kinetic energy variations were neglected and no heat loss from the pipes or equipment was considered, except for the storage tanks and solar collectors.

3.1. Optimization

The economic objective function could be selected from the internal rate of return (IRR), net present value (NPV) and levelized cost of energy (LCOE). The optimization was carried out considering binary variables to represent technology selection and continuous variables that were related to the power block mass flow rate ($\dot{m}_{PB}$), heat source inlet (T_H) and outlet (T_C) temperatures and the TES storage capacity, as well as the continuous

design variables that were related to the aperture and heat transfer areas. Table 1 shows the decision variables and their upper and lower bounds, in which S represents the binary structure decision variables, A represents the aperture or heat transfer areas and i is a counter representing any chosen waste heat source or collector type.

Table 1. Lower and upper bounds of the hybrid solar–waste heat power plant decision variables.

Variable	Description	Type	Lower Bound	Upper Bound
S_i; $1 \leq i \leq 6$	Structure Decision Variables	Binary	0	1
A_i; $1 \leq i \leq 6$	Aperture or Heat Exchanger Areas	Continuous	0 m	1×10^6 m
$\dot{Q}_{PB}$	Heat Transfer Rate to PB	Continuous	100 kW	50,000 kW
T_H	PB Inlet Temperature	Continuous	106 °C	350 °C
T_C	PB Outlet Temperature	Continuous	96 °C	340 °C
t_{TES}	TES Storage Capacity	Continuous	0 h	12 h

Simultaneous to the hybrid field optimization, the power block and storage tanks were optimized using surrogate models, which are described in their respective sections.

A genetic algorithm from jMetalPy [26] was used for optimization. A modification to the population of the first generation using a Latin hypercube stratification (LHS) for the continuous variables and all possible combinations of the binary variables was used in order to improve the quality of the first population.

Algorithm Logic

The hybrid solar field could be operated according to the following modes, depending on the local time-dependent irradiance: (i) loading the hot tank; (ii) loading the hot tank and running the ORC; or (iii) running the ORC with the help of the hot tank. The operation mode was selected by the optimization algorithm for every hour of the specified period of time.

The hourly HSF mass flow rate ($\dot{m}_{HSF}$) was calculated using Equation (1) as a function of the sum of the heat provided by the heat exchangers ($\dot{Q}_{WHR}$) and solar collectors ($\dot{Q}_{col}$) and the thermal fluid enthalpies, i.e., it was a function of the decision variables that were under selection.

$$\dot{m}_{HSF} = \frac{\sum \dot{Q}_{col} + \sum \dot{Q}_{WHR}}{h_H - h_C} \tag{1}$$

The power block mass flow rate ($\dot{m}_{PB}$) was calculated by adding $\dot{m}_{HSF}$ to the mass flow rate from the tank level variation ($\dot{m}_{TES}$), see Equation (2). When $\dot{m}_{TES}$ was negative in Equation (2), the HSF was supplying the PB and charging the TES at the same time. When $\dot{m}_{HSF} + \dot{m}_{TES}$ was not enough to meet the power block design flow rate, it was turned off.

$$\dot{m}_{PB} = \dot{m}_{HSF} + \dot{m}_{TES} \tag{2}$$

Figure 2 shows the algorithm flowchart, which includes the optimization block and the thermodynamic block. Firstly, the algorithm read the input data, which was composed of economic and historic climate information as well as the avaliable collectors and waste heat characterisctics that were selected by the user. Then, it defined the typical meteorological period (the user could choose between 1, 4, 12 or 52 typical days or a whole typical year; however, for the sake of simplicity, Figure 2 is for one typical day) to compress the historical climate input and the number of possible combinations of collectors and waste heat sources

as well as the LHS stratification of the decision variables. The optimization block defined the decision variables, i.e., the configuration and sizing of the HSF, the tank capacity and the power block operational point ($\dot{m}_{PB}$, T_H and T_C), which were assigned to every individual that was provided by the genetic algorithm. The thermodinamic block, in turn, defined the best power block for the selected operational point based on its surrogate model and then calculated the hourly mass flow and the TES heat loss to define the power block status at each hour of the selected typical period.
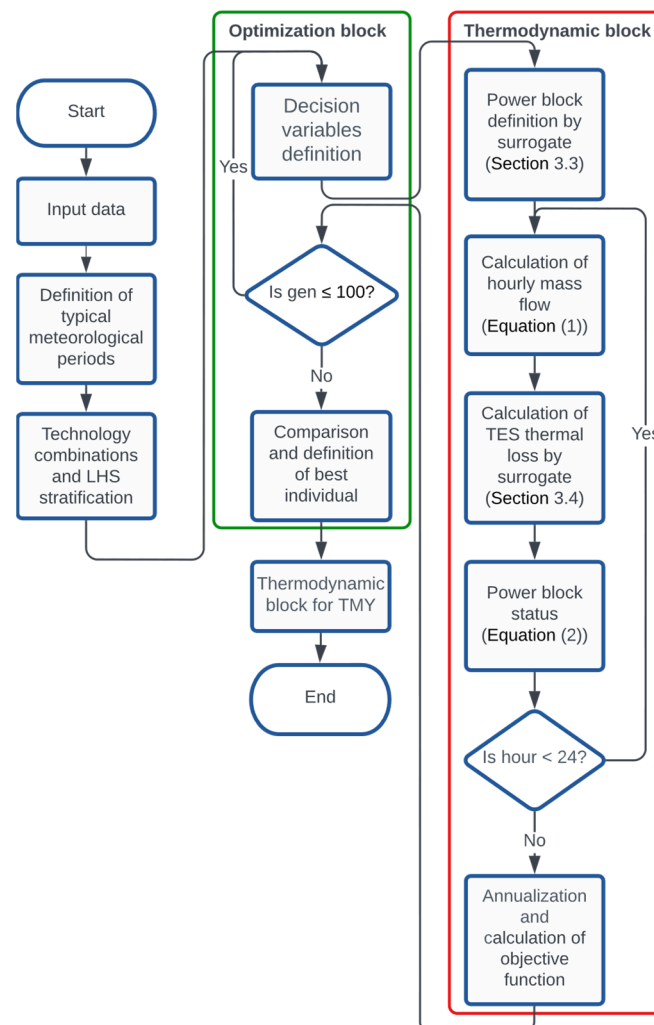
Figure 2. The algorithm flowchart for a typical day.

The loop inside the thermodynamic block indicated that the ORC only worked under design conditions. When there was not enough energy for that, the hybrid field mass flow rate was decreased to keep its temperature constant, the ORC was turned off and the energy was stored in the hot tank. This stored energy was then used when there was enough to run the ORC under design conditions for at least one hour.

Then, the daily result was annualized in order to calculate the objective function result based on the lifespan of the plant.

3.2. Hybrid Solar–Waste Heat Field

Tubular heat exchangers were selected to make use of the waste heat. Their sizing was based on the overall heat transfer coefficient (U) and the logarithmic mean temperature dif-

ference (T_{LM}), see Equation (3). The overall heat transfer coefficient was calculated based on the cold and hot side convective coefficients and the fouling resistances, as presented in [27].

$$\dot{Q}_{WHR} = UAT_{mean} \tag{3}$$

The solar collector energy balance was related to the amount of solar energy that was converted into thermal energy and delivered to the heat transfer fluid (HTF), see Equation (4). In this equation, $\dot{m}_{HTF}$ is the HTF mass flow rate, $\eta_{C,t}$ is the collector thermal efficiency, I_s is the solar irradiance and A is the collector aperture area. For non-concentrating solar collectors, I_s is the global horizontal irradiance (GHI) and for concentrating collectors, I_s is the direct normal irradiance (DNI).

$$\eta_{C,t} I_s A = \dot{m}_{HTF}(h_{HTF,out} - h_{HTF,in}) \tag{4}$$

The collector thermal efficiency ($\eta_{C,t}$) was calculated based on (i) the optical losses due to the incidence angle, which is represented by the incidence angle modifier (IAM), (ii) the collector optical efficiency ($\eta_{C,\,opt}$) and (iii) the thermal energy loss, which is generally represented by the overall heat loss coefficient (U_L), see Equation (5) [7,8].

$$\eta_{C,t} = IAM\eta_{C,opt} - \frac{U_L}{I_s A}(T_{HTF} - T_{amb}) \tag{5}$$

The IAM and U_L values depend on the specific collector and can take local wind speed into account. The detailed formulation of these coefficients can be found in [28,29] for non-concentrating solar collectors, in [30,31] for linear Fresnel collectors and in [32,33] for parabolic trough collectors.

3.3. Power Block

The power block (PB) was based on organic Rankine cycle (ORC) technology. It was optimized in terms of structure, operational condition, heat transfer fluid and working fluid as a function of the heat transfer rate and heat source inlet and outlet temperatures, i.e., the decision variables of the power block, its working fluid and configuration change during optimization for each hybrid field that was tested. Four structures were considered: (i) a subcritical ORC, (ii) a subcritical recuperative ORC, (iii) a supercritical ORC and (iv) a supercritical recuperative ORC. Moreover, the six most commonly used commercial working fluids (D4, R134a, R245fa, ammonia, R1233zd and SES36) [34,35] and two heat transfer fluids (Dowtherm A and Syltherm 800) [36,37] were evaluated. Since the plate heat exchanger dimensions and fluid velocity were also decision variables, the pressure loss was restricted to avoid unrealistic configurations. Furthermore, due to the nature of dry fluids, condensation could occur inside the turbine during the expansion, even when its state at the end of expansion was superheated steam. Thus, the steam quality was assured by dividing the expansion into 10 constant pressure drop steps and checking the quality of the steam for each of them.

Each combination of structure, working fluid and heat transfer fluid was optimized in terms of its operational conditions by applying the jMetalPy [26] genetic algorithm (GA) using the decision variables and constraints that are shown in Table 2 [38]. Since the power block model was too complex to run for each hybrid field under selection (at each loop), a surrogate approach was used, i.e., a large number of inputs and outputs were generated and those points were used to create a simpler function that mimicked the thermodynamic and economic model. More details on this procedure can be found in [38].

Table 2. Lower and upper bounds of the optimized ORC decision variables.

Variable	Type	Lower Bound	Upper Bound
Evaporation Pressure	Decision Variable	4.01325 bar	42 bar
Condensation Pressure	Decision Variable	1.01325 bar	Working Fluid Critical Pressure
Turbine Inlet Temperature	Decision Variable	Condensation Temperature	Source Inlet Temperature
Recuperator Outlet Temperature at Cold Side	Decision Variable	Condensation Temperature	Source Outlet Temperature
Evaporator Plate Width	Decision Variable	0.3048 m	4.572 m
Condenser Plate Width	Decision Variable	0.3048 m	4.572 m
Recuperator Plate Width	Decision Variable	0.3048 m	4.572 m
Evaporator Working Fluid Velocity	Decision Variable	0.2 m/s	2.0 m/s
Condenser Working Fluid Velocity	Decision Variable	0.2 m/s	2.0 m/s
Recuperator Working Fluid Velocity	Decision Variable	0.2 m/s	2.0 m/s
Pinch Point Temperature Difference	Constraint	4 °C	-
Turbine Pressure Difference	Constraint	3 bar	-
Quality During Expansion	Constraint	0.8	-
Heat Exchanger Pressure Drop	Constraint	0	1.8 bar

3.4. Storage Tank Heat Loss

Figure 3 shows the heat loss mechanisms that were considered, i.e., radiation (r), convection (c) and conduction (k), in each part of the tank. The ambient temperature was available hourly and the foundation temperature was maintained below 90 °C using a cooling system to avoid cracking, as indicated in [39]. The tank insulation thickness followed the Petrobras technical standard N-550 [40], which relates the insulation thickness to the tank diameter and its operational temperature. The NBR 7821 standard [41] was used to define the thickness of the tank's steel sheets.
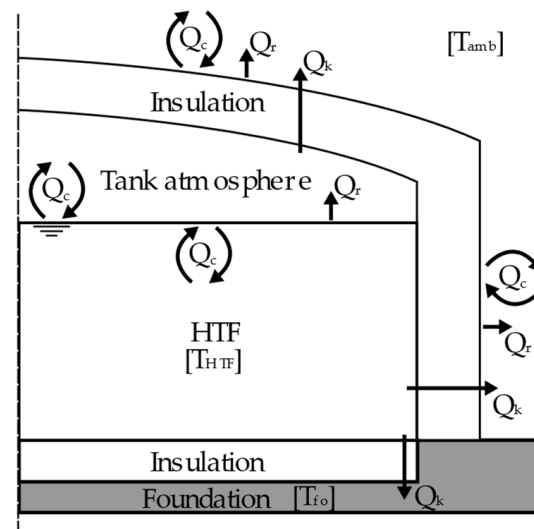
Figure 3. The TES thermal loss mechanisms (adopted from [39,42]).

The model developed was compared to the work in [43,44] and differences of between 1.0% and 27.0% were found for different operational conditions. The differences were probably caused by the indirect methodology that was used to define the storage tank heat loss in those works, such as the time required for the temperature of the fluid inside tank to decrease by 1 °C and the power required to keep the fluid temperature constant. Since the tank models had to run for each hybrid field under selection, such as for the power block, a surrogate approach was used to replace the thermodynamic and economic model with a simpler model that could provide similar results.

3.5. Local Irradiance Data

A typical meteorological year (TMY) was used to compress the information of large historical periods. The months that comprised the TMY were selected as the best representatives for the period of time that was available for assessment on the NREL website, which is usually many years, considering the smallest Finkesltein–Schafer (FS) statistical distances for each weather characteristic, as indicated in [45]. The same concept was applied to define a typical meteorological day (TMD), so that the entire period could be condensed within a typical day. It is important to stress that not only are average values important, but the sequences of values over the hours are also essential to quantify the amount of stored energy and the TES loss and to estimate the collector thermal efficiency and absorbed energy. Even though the hourly irradiation of a typical day (24 h) was used to choose the best configuration using the developed program, the final result of the chosen configuration was calculated using all of the hours in a typical year (8760 h), which is emphasized later in the results section.

3.6. Economic Model

The plant costs were separated into (i) capital expenditure (CAPEX) and (ii) operational expenditure ($OPEX$). The CAPEX represented the purchase equipment cost (PEC), transportation, taxes and installation. The cost of all components was given according to Equation (6), as proposed by Bejan et al. [46]. The pressure factor (f_p) and material factor (f_m) were assumed to be 1 and X was the equipment capacity. The Chemical Engineering Plant Cost Index ($CEPCI$) was used to correct previous quotations by taking inflation or deflation into account. The reference cost (C_{ref}), reference capacity (X_{ref}) and exponent α were obtained using Thermoflex® [47] and System Advisor Model (SAM) [48] data. The total PEC was obtained as a sum of each equipment cost.

$$C = f_{int} f_p f_m C_{ref} \left(\frac{X}{X_{ref}} \right)^{\alpha} \left(\frac{CEPCI}{CEPCI_{ref}} \right) \tag{6}$$

The CAPEX was calculated as the sum of direct costs (DCs) and indirect costs (ICs). Both direct (Equation (7)) and indirect costs (Equation (8)) were obtained from the PEC by adding the multipliers and were expressed as a percentage of the total PEC [46]. Table 3 describes each of those coefficients.

$$DC = (1 + p_{HTF} + p_{PEI} + p_{PP} + p_{IC} + p_{EEM} + p_{CSAW} + p_{SF})PEC \tag{7}$$

$$IC = (p_{ES} + 1)p_{CON}DC \tag{8}$$

Table 3. Cost multipliers that were used in the CAPEX calculation.

Variable	Description	Value	Reference
p_{HTF}	HTF Costs	20%	[48]
p_{EI}	Equipment Installation Costs	30%	[46]
p_P	Piping Costs	20%	[46]
p_{IC}	Instrumentation and Control Costs	30%	[46]
p_{EE}	Electrical Equipment Costs	10%	[46]
p_{CSA}	Civil, Structural and Architectural Costs	10%	[46]
p_{SF}	Service Facilities Costs	40%	[46]
p_{ES}	Engineering and Supervisor Costs	10%	[46]
p_{CON}	Contingences	10%	[46]

Equation (9) was used to determine the plant's operation and maintenance costs ($OPEX$). A fixed $OPEX$ cost ($C_{OPEX,fix}$) that was related to the plant's installed capacity

(W_{PB}) and a variable *OPEX* cost ($C_{OPEX,var}$) that was related to the net generated energy ($E_{net,year}$) were considered.

$$OPEX = C_{OPEX,fix}\dot{W}_{PB} + C_{OPEX,var}E_{net,year} \tag{9}$$

4. Case Study

A typical diesel engine exhaust gas (74.7% N_2, 13.9% O_2, 8.5% CO_2 and 2.9% H_2O on mass basis) was considered as the waste heat and Candeias (-12.73 N, -38.48 L) was considered as the location. In order to cover different applications, the waste heat power ranged from 100 kWt to 50 MWt and its temperature ranged from 150 °C to 350 °C. These values were selected to meet the power block model limits [38]. Table 4 summarizes the main characteristics of the specific collectors that were considered (user input) for algorithm selection during optimization, aiming at the maximum internal rate of return (IRR) (objective function selected by the user).

Table 4. Characteristics of the selected collectors.

Collector Type	Manufacturer	Model	Maximum Operating Temperature	Reference
Flat Plate	SolarTEK	ST400	208 °C	[48]
Evacuated Tube	Kingspan Solar Inc.	Thermomax DF100-30	300 °C	[48]
Linear Fresnel	Industrial Solar	LF-11	400 °C	[49]
Parabolic Trough	SkyFuel (Reflector) Solel (Receiver)	SkyTrough (Reflector) UVAC3 (Receiver)	560 °C	[48]

The values of the cost multipliers are shown in Table 3. An extra internalization factor (f_{int}) of 1.2 and 2 for the power block and collectors, respectively, was considered to cover taxes and additional structural construction costs (wind barriers, trackers, etc.). A lifespan (Y) of 20 years, $C_{OPEX,fix}$ and $C_{OPEX,var}$ of 66 USD/kWe and 4 USD/MWhe [48], respectively, and a long-term inflation rate (π) of 3% per year [50] were considered.

Additionally, three real waste heat sources near the selected area were analyzed: two reciprocating engine exhaust gases and a surplus of saturated steam.

5. Results and Discussion

The convergence of the genetic algorithm was tested experimentally and 100 generations were used. Nevertheless, a tool for the graphic visualization of the convergence, i.e., generation number vs. objective function, allowed the user to infer whether there was convergence or not. Figure 4 shows the IRR for the range of temperature and thermal power that was considered. The use of a waste heat source, i.e., a heat exchanger to recover the waste heat with no collectors or TES selected, was the best option for all cases, except for 0.1 MWt of waste heat. For the case of 0.1 MWt of waste heat at 150 °C, a PTC field and TES were selected (no use of waste heat) due to the low quality of the waste heat, i.e., low exergy caused by low temperature. The algorithm was free to select any of the four collectors (or combinations of the collectors) during optimization. However, probably due to its good ratio of price to performance, the parabolic trough collector was the only option chosen. For 0.1 MWt of waste heat at higher temperatures, the waste heat and TES were selected without a collector. The TES was used to supply the extra thermal power that was required by the power block, for which the minimum power input after all heat exchanges was 0.1 MWt (see Table 1). Furthermore, the 0.1 MWt line was the only one with technologies that were dependent on climate condition, i.e., solar collectors and/or TES (TES heat loss depends on local temperature while solar collectors depend on local temperature and wind velocity).
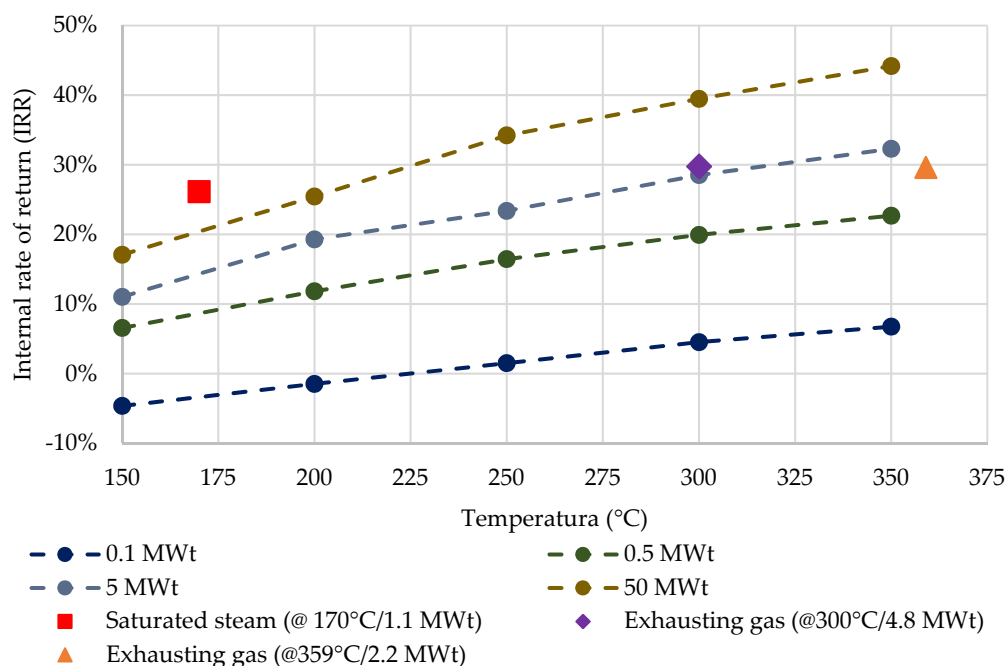
Figure 4. The optimized IRR values.

The isolated points in Figure 4 represent the real waste heat sources near the selected area. The saturated steam (red square at 170 °C/1.1 MWt), exhaust gas (orange triangle at 359 °C/2.2 MWt) and the second exhaust gas (purple rhombus at 300 °C/4.8 MWt) provided 0.13 USD/kWhe, 0.11 USD/kWhe and 0.11 USD/kWhe of LCOE, respectively, at their optimum IRR. Only the waste heat and ORC were selected by the algorithm for these cases. It should be noted that the saturated steam provided a high IRR, despite its low temperature. This happened due to its higher overall heat transfer coefficient (U), which was 3.6 times higher than the U value of the other two cases.

Figure 5 shows the response of the IRR to the electricity price for the three real cases and for the lowest point at Figure 4. The vertical lines over the bars in Figure 5 represent the amplitude of the IRR when the energy price increased or decreased by 50%. The results show that, despite the variations in energy price, PTC as a single thermal source was the best choice when the waste heat was at 150 °C and 100 kWt. The IRR remained non-competitive though, reaching a maximum of 0% when the energy price increased. For solar collectors, the variations in energy price caused a variation in the IRR of around ±4.7%. The waste heat sources, in turn, presented greater variations in the IRR when the energy price decreased (−16.6% on average) compared to the variations when the energy price increased (+11.3% on average). In these cases, when the energy price increased, the optimization converged to a power plant that was similar to that selected under the original price conditions, but when the energy cost decreased, the plant operational and design variables were very different from those that were selected under the original price conditions. This increased the power block-specific costs and decreased the plant's installed capacity.

Comparisons of different typical periods of time are plotted in Figure 6: (a) a comparison of the results of a typical day and the results of using a typical day for technology selection and a typical year for final result, i.e., once the technology was selected using one typical day (24 h) and it was then evaluated under the climate conditions provided for an entire typical year (8760 h); (b) a comparison of the results of a period composed of four typical days (one for each season) and the results of using four typical days for technology selection and a typical year for the final result; and (c) a comparison of the results of technology selection using a typical day and the application of a typical year to obtain the final results and the results of using four typical days for technology selection

and the application of a typical year to obtain the final results. The maximum difference in the IRR in this last case was 0.3%. This meant that the selection of technology was less sensitive to the typical period used than the final result, but a significant reduction in computational time was obtained due to the reduction from four typical days (5.8 h) to a single typical day (1.2 h) for the technology selection (results obtained using an i5-10400F with 4.3 GHz, 6 cores and 12 threads).
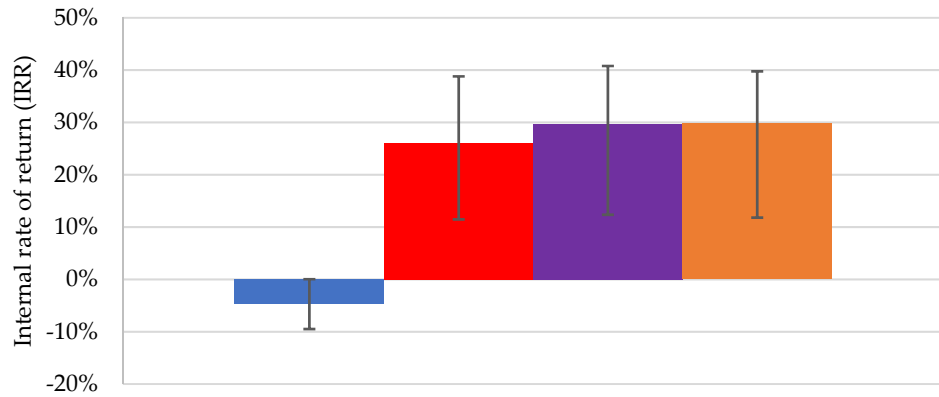

Figure 5. The energy price sensitivity analysis.
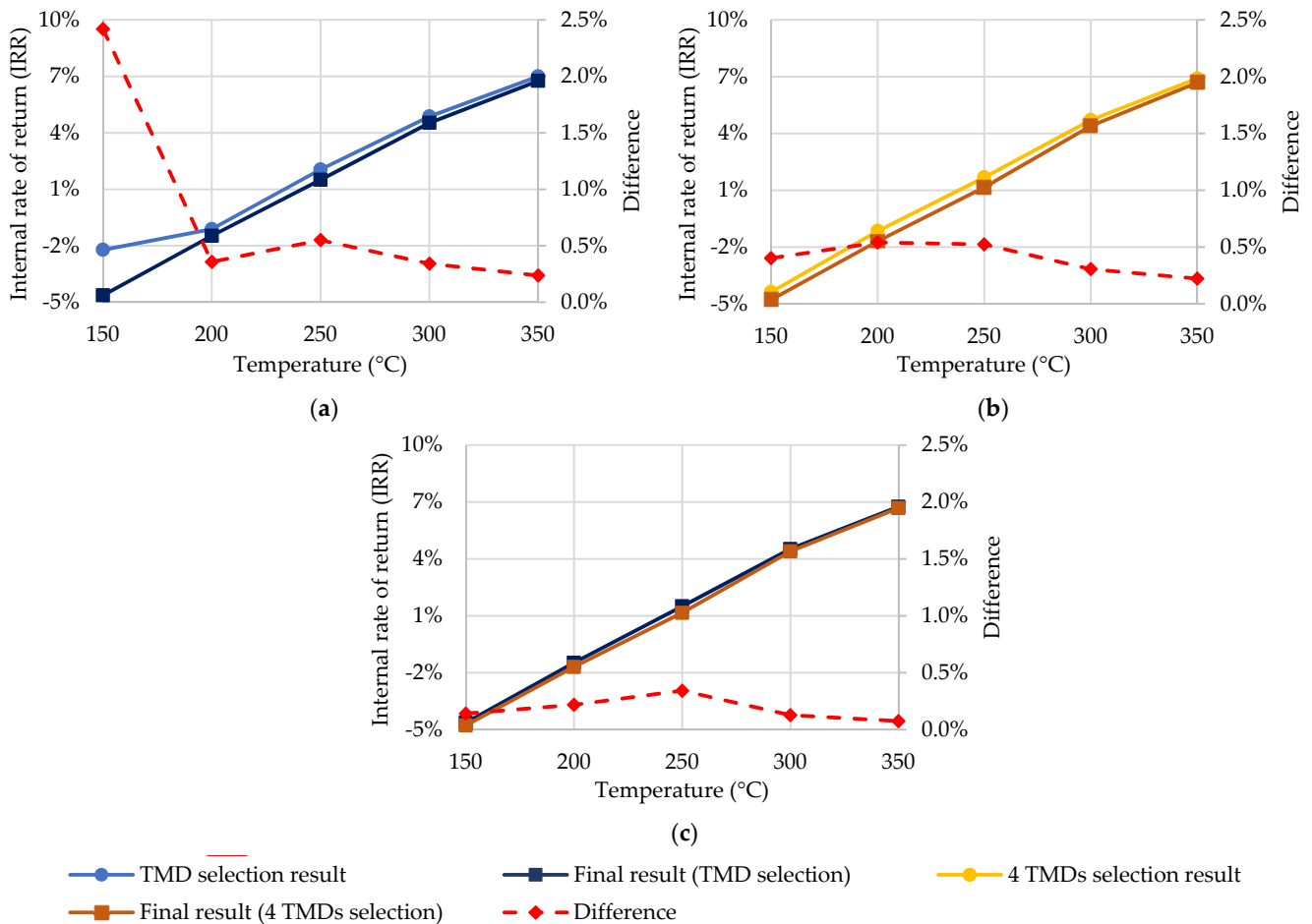
Figure 6. Comparison between the IRRs of the optimized plants for (**a**) a single TMD and (**b**) four TMDs and (**c**) the TMY for results for a single TMD and four TMDs.

All in all, heliothermic technologies were still not economically competitive in the studied cases and presented negative IRRs. On the other hand, the optimized ORCs seemed to be very competitive, depending on the waste heat characteristics.

6. Conclusions

A comprehensive software for the economic optimization of hybrid solar–waste heat power systems was developed in this study. The structure, sizing and operational conditions were optimized in order to maximize the economic indicator (IRR, NPV or LCOE) that was chosen by the user. While real models (thermodynamic and economic) were used for the hybrid field components, surrogate models were used for the power block and storage tanks so that a large number of free variables could be optimized simultaneously, without impeditive computational burdens.

A case study using a waste heat power ranging from 0.1 to 50 MWt and a temperature ranging from 150 to 300 °C was created and four types of solar collectors were available for algorithm selection. PTC technology was the only collector selected. Additionally, it was only selected for the point with the lowest power and temperature combination, i.e., 0.1 MWt and 150 °C. For all other combinations, the waste heat was the only energy source selected. The IRR seemed to be more sensitive to a decrease in electricity price than to an increase. The use of a typical day for technology selection while the final results were calculated using all of the hours in a typical year proved to be a reasonable strategy to reduce computational time (79%) without significant reductions in precision (0.3%) during the IRR optimization.

Heliothermic technology was not economic competitive under the conditions proposed in the case study, even when the possibility of hybridization with waste heat was present. Optimized ORCs for waste heat recovery, on the other hand, were very competitive with internal rates of return of 44%, 39% and 34% for 50 MWt of waste heat at 350 °C, 300 °C and 250 °C, respectively. For the three real local waste heat considered, i.e., saturated steam (170 °C/1.1 MWt), exhaust gas (300 °C/4.8 MWt) and the second exhaust gas (350 °C/2.2 MWt), the IRRs were 26%, 30% and 30%, respectively, while the LCOE ranged from 0.11 USD/kWhe to 0.13 USD/kWhe.

References

1. Kalogirou, S.A. Solar Thermal Collectors and Applications. *Prog. Energy Combust. Sci.* **2004**, *30*, 231–295. [CrossRef]
2. U. S. Energy Information Administration. International Energy Outlook 2019. *Choice Rev. Online* **2019**, *85*, 169.
3. la Rocca, V.; Morale, M.; Peri, G.; Scaccianoce, G. A Solar Pond for Feeding a Thermoelectric Generator or an Organic Rankine Cycle System. *Int. J. Heat Technol.* **2017**, *35*, S435–S441. [CrossRef]

4. Shamsi, H.; Boroushaki, M.; Geraei, H. Performance Evaluation and Optimization of Encapsulated Cascade PCM Thermal Storage. *J. Energy Storage* **2017**, *11*, 64–75. [CrossRef]

5. Price, H.; Carpenter, S. The Potential for Low-Cost Electricity from Concentrating Solar Power Systems. In Proceedings of the 34th Intersociety Energy Conversion Engineering Conference, Vancouver, BC, Canada, 2–5 August 1999.

6. Herrmann, U.; Kearney, D.W. Survey of Thermal Energy Storage for Parabolic Trough Power Plants. *J. Sol. Energy Eng.* **2002**, *124*, 145–152. [CrossRef]

7. Duffie, J.A.; Beckman, W.A. *Solar Engineering of Thermal Processes*, 4th ed.; John Wiley & Sons, Inc.: Hoboken, NJ, USA, 2013; ISBN 9781118671603.

8. Kalogirou, S.A. *Solar Energy Engineering: Processes and Systems*, 2nd ed.; Elsevier Inc.: Oxford, UK, 2014; ISBN 9780123972705.

9. Mendecka, B.; Lombardi, L.; Gładysz, P.; Stanek, W. Exergo-Ecological Assessment of Waste to Energy Plants Supported by Solar Energy. *Energies* **2018**, *11*, 773. [CrossRef]

10. Franchini, G.; Perdichizzi, A.; Ravelli, S.; Barigozzi, G. A Comparative Study between Parabolic Trough and Solar Tower Technologies in Solar Rankine Cycle and Integrated Solar Combined Cycle Plants. *Sol. Energy* **2013**, *98*, 302–314. [CrossRef]

11. Rashid, K.; Safdarnejad, S.M.; Ellingwood, K.; Powell, K.M. Techno-Economic Evaluation of Different Hybridization Schemes for a Solar Thermal/Gas Power Plant. *Energy* **2019**, *181*, 91–106. [CrossRef]

12. Chen, H.; Wu, Y.; Zeng, Y.; Xu, G.; Liu, W. Performance Analysis of a Solar-Aided Waste-to-Energy System Based on Steam Reheating. *Appl. Therm. Eng.* **2021**, *185*, 116445. [CrossRef]

13. Arabkoohsar, A.; Sadi, M. Thermodynamics, Economic and Environmental Analyses of a Hybrid Waste–Solar Thermal Power Plant. *J. Therm. Anal. Calorim.* **2021**, *144*, 917–940. [CrossRef]

14. Han, Y.; Sun, Y.; Wu, J. A Low-Cost and Efficient Solar/Coal Hybrid Power Generation Mode: Integration of Non-Concentrating Solar Energy and Air Preheating Process. *Energy* **2021**, *235*, 121367. [CrossRef]

15. Behar, O.; Khellaf, A.; Mohammedi, K.; Ait-Kaci, S. A Review of Integrated Solar Combined Cycle System (ISCCS) with a Parabolic Trough Technology. *Renew. Sustain. Energy Rev.* **2014**, *39*, 223–250. [CrossRef]

16. Brodrick, P.G.; Brandt, A.R.; Durlofsky, L.J. Operational Optimization of an Integrated Solar Combined Cycle under Practical Time-Dependent Constraints. *Energy* **2017**, *141*, 1569–1584. [CrossRef]

17. Pantaleo, A.M.; Camporeale, S.M.; Sorrentino, A.; Miliozzi, A.; Shah, N.; Markides, C.N. Hybrid Solar-Biomass Combined Brayton/Organic Rankine-Cycle Plants Integrated with Thermal Storage: Techno-Economic Feasibility in Selected Mediterranean Areas. *Renew. Energy* **2020**, *147*, 2913–2931. [CrossRef]

18. Alirahmi, S.M.; Rahmani Dabbagh, S.; Ahmadi, P.; Wongwises, S. Multi-Objective Design Optimization of a Multi-Generation Energy System Based on Geothermal and Solar Energy. *Energy Convers. Manag.* **2020**, *205*, 112426. [CrossRef]

19. de Araújo Coutinho, D.P.; Rodrigues, J.A.M.M.; dos Santos, A.J.P.; de Almeida Semiao, V.S. Thermoeconomic Analysis and Optimization of a Hybrid Solar-Thermal Power Plant Using a Genetic Algorithm. *Energy Convers. Manag.* **2021**, *247*, 114669. [CrossRef]

20. Elmorsy, L.; Morosuk, T.; Tsatsaronis, G. Exergy-Based Analysis and Optimization of an Integrated Solar Combined-Cycle Power Plant. *Entropy* **2020**, *22*, 655. [CrossRef]

21. Rovira, A.; Abbas, R.; Muñoz, M.; Sebastián, A. Analysis of an Integrated Solar Combined Cycle with Recuperative Gas Turbine and Double Recuperative and Double Expansion Propane Cycle. *Entropy* **2020**, *22*, 476. [CrossRef]

22. Witte, F.; Tuschy, I. TESPy: Thermal Engineering Systems in Python. *J. Open Source Softw.* **2020**, *5*, 2178. [CrossRef]

23. Pedregosa, F.; Varoquaux, G.; Gramfort, A.; Michel, V.; Thirion, B.; Grisel, O.; Blondel, M.; Prettenhofer, P.; Weiss, R.; Dubourg, V.; et al. Scikit-Learn: Machine Learning in Python. *J. Mach. Learn. Res.* **2011**, *12*, 2825–2830.

24. Bell, I.H.; Wronski, J.; Quoilin, S.; Lemort, V. Pure and Pseudo-Pure Fluid Thermophysical Property Evaluation and the Open-Source Thermophysical Property Library CoolProp. *Ind. Eng. Chem. Res.* **2014**, *53*, 2498–2508. [CrossRef] [PubMed]

25. Sengupta, M.; Xie, Y.; Lopez, A.; Habte, A.; Maclaurin, G.; Shelby, J. The National Solar Radiation Data Base (NSRDB). *Renew. Sustain. Energy Rev.* **2018**, *89*, 51–60. [CrossRef]

26. Benítez-Hidalgo, A.; Nebro, A.J.; García-Nieto, J.; Oregi, I.; del Ser, J. JMetalPy: A Python Framework for Multi-Objective Optimization with Metaheuristics. *Swarm Evol. Comput.* **2019**, *51*, 100598. [CrossRef]

27. Bell, K.J. Shell-and-Tube Heat Exchangers. In *The CRC Handbook of Thermal Engineering*; Kreith, F., Ed.; CRC Press LLC: Boca Raton, FL, USA, 2000.

28. Goswami, D.Y. *Principles of Solar Engineering*, 3rd ed.; CRC Press: Boca Raton, FL, USA, 2015; ISBN 9781466563797.

29. Thomas, W.C.; Dawson, A.G.; Waksman, D.; Streed, E.R. Incident Angle Modifiers for Flat-Plate Solar Collectors: Analysis of Measurement and Calculation Procedures. *J. Sol. Energy Eng.* **1982**, *104*, 349–357. [CrossRef]

30. Wagner, M.J. Results and Comparison from the SAM Linear Fresnel Technology Performance Model: Preprint. In Proceedings of the 2012 World Renewable Energy Forum, Denver, CO, USA, 13–17 May 2012.

31. Wagner, M.J.; Zhu, G. A Direct-Steam Linear Fresnel Performance Model for NREL's System Advisor Model. In Proceedings of the ASME 2012 6th International Conference on Energy Sustainability Collocated with the ASME 2012 10th International Conference on Fuel Cell Science, Engineering and Technology, San Diego, CA, USA, 23–26 July 2012.

32. Price, H. A Parabolic Trough Solar Power Plant Simulation Model. In Proceedings of the ASME 2003 International Solar Energy Conference, Kohala Coast, HI, USA, 15–18 March 2003.

33. Burkholder, F.; Kutscher, C. *Heat Loss Testing of Schott's 2008 PTR70 Parabolic Trough Receiver*; National Renewable Energy Lab: Golden, CO, USA, 2009.
34. Quoilin, S.; van den Broek, M.; Declaye, S.; Dewallef, P.; Lemort, V. Techno-Economic Survey of Organic Rankine Cycle (ORC) Systems. *Renew. Sustain. Energy Rev.* **2013**, *22*, 168–186. [CrossRef]
35. Dincer, I.; Zamfirescu, C. Conventional Power Generating Systems. In *Advanced Power Generation Systems*; Elsevier: Amsterdam, The Netherlands, 2014; pp. 199–310.
36. Moens, L.; Blake, D.M. Advanced Heat Transfer and Thermal Storage Fluids. In Proceedings of the ASME 2005 International Solar Energy Conference, Orlando, FL, USA, 6–12 August 2005.
37. Jiménez-Arreola, M.; Wieland, C.; Romagnoli, A. Direct vs. Indirect Evaporation in Organic Rankine Cycle (ORC) Systems: A Comparison of the Dynamic Behavior for Waste Heat Recovery of Engine Exhaust. *Appl. Energy* **2019**, *242*, 439–452. [CrossRef]
38. Vilasboas, I.F.; dos Santos, V.G.S.F.; Ribeiro, A.S.; da Silva, J.A.M. Surrogate Models Applied to Optimized Organic Rankine Cycles. *Energies* **2021**, *14*, 8456. [CrossRef]
39. Zaversky, F.; García-Barberena, J.; Sánchez, M.; Astrain, D. Transient Molten Salt Two-Tank Thermal Storage Modeling for CSP Performance Simulations. *Sol. Energy* **2013**, *93*, 294–311. [CrossRef]
40. Petrobras. *N-550: Projeto de Isolamento Térmico a Alta Temperatura*; CONTEC: Rio de Janeiro, Brazil, 1995.
41. ABNT. *NBR 7821: Tanques Soldados Para Armazenamento de Petróleo e Derivados*; ABNT: Rio de Janeiro, Brazil, 1983.
42. Araújo, A.K.A.; Medina, T.G.I. Analysis of the Effects of Climatic Conditions, Loading Level and Operating Temperature on the Heat Losses of Two-Tank Thermal Storage Systems in CSP. *Sol. Energy* **2018**, *176*, 358–369. [CrossRef]
43. Pacheco, J.E.; Bradshaw, R.W.; Dawson, D.B.; De la Rosa, W.; Gilbert, R.; Goods, S.H.; Hale, M.J.; Jacobs, P.; Jones, S.; Kolb, G.; et al. Final Test and Evaluation Results from the Solar Two Project. *Contract* **2002**, 294. [CrossRef]
44. National Renewable Energy Laboratory. Andasol 1 CSP Project. Available online: https://solarpaces.nrel.gov/project/andasol-1 (accessed on 24 July 2021).
45. Wilcox, S.; Marion, W. Users Manual for TMY3 Data Sets. 2008. Available online: https://www.nrel.gov/docs/fy08osti/43156.pdf (accessed on 4 April 2022).
46. Bejan, A.; Tsatsaronis, G.; Moran, M. *Thermal Design and Optimization*, 1st ed.; John Wiley & Sons, Inc.: Hoboken, NJ, USA, 1995; ISBN 978-0-471-58467-4.
47. Thermoflow Inc. *Thermoflex*; Thermoflow Inc.: Jacksonville, FL, USA, 2021.
48. National Renewable Energy Laboratory. System Advisor Model 2021. Available online: https://sam.nrel.gov/ (accessed on 20 April 2022).
49. Industrial Solar. *Industrial Solar Fresnel Collector LF-11 Datasheet 1–3*; Industrial Solar: Freiburg, Germany, 2020.
50. Banco Central do Brasil. Focus-Market Readout. 2022. Available online: https://www.bcb.gov.br/en/publications/focusmarketreadout (accessed on 5 April 2022).